International Journal of Thermophysics, Vol. 17, No. 5, 1996

Measurements of Thermophysical Properties by Contactless Modulation Calorimetry[1]

R. K. Wunderlich[2, 3] and H.-J. Fecht[2]

Contactless modulation calorimetry was applied to measure the specific-heat of glass forming eutectic Zr alloys in the stable and undercooled liquid under microgravity conditions during the space shuttle IML-2 mission. The experimental method is described, leading to a quantitative determination of the specific heat from measured temperature modulations. In addition, the enthalpy of fusion of the specimen and the total hemispherical emissivity can be obtained. The data on $ZrNi_{36}$ permit calculation of the thermodynamic functions in the stable and undercooked melt as well as estimation of the ideal glass transition temperature.

KEY WORDS: containerless processing; metallic glasses; modulation calorimetry; undercooled melts.

1. INTRODUCTION

The transient thermal response of a specimen exposed to variable heat input is dependent on thermophysical properties such as the specific heat, thermal conductivity, thermal conductances to a heat bath, and measuring devices and on the enthalpy and kinetics of phase transformations. Modulation calorimetry applied in a suitable range of modulation frequencies permits separation of the influence of the different thermal relaxation times on the thermal response of a specimen exposed to modulated heating power input and, as such, allows direct determination of the specific heat from measured temperature variations [1–6]. This requires that the amplitude of power modulation in the temperature range of interest can be

[1] Paper presented at the Fourth International Workshop on Subsecond Thermophysics, June 27–29, 1995, Köln, Germany.

[2] Institut für Metallforschung–Metallphysik, Technische Universität Berlin, Hardenbergstr. 36, PN2-3, 10623 Berlin, Germany.

[3] To whom correspondence should be addressed.

0195-928X/96/0900-1203$09.50/0

accurately determined and that the relevant thermal relaxation times differ sufficiently from the modulation time scale. Typically, the latter condition is met in levitated metallic specimens because of the large difference in the rates of radiative heat loss and thermal transport within the specimen.

Containerless processing conditions are relevant for the study of undercooling and nucleation phenomena [7]. In particular, thermophysical investigations of metallic glass forming alloys depend on the availability of a stable undercooked melt over a time scale sufficient to perform measurements of, e.g., the specific heat, thermal expansion, surface tension, and viscosity. A knowledge of the specific heat in the undercooked melt permits calculation of the thermodynamic functions ΔG^{lx}, ΔS^{lx}, and ΔH^{lx}, from which the reduced glass transition temperature T_{go}/T_m indicative of the glass forming tendency of a specific alloy, can be evaluated. Here Δ^{lx} refers to the difference between liquid and solid phase. Combined with viscosity data [8], these results can be used for modeling of nucleation kinetics [9, 10]. However, due to the high chemical reactivity of many specimens with their surroundings at high temperatures and the dominance of heterogeneous nucleation in conventional processing techniques, thermophysical property measurements at temperatures $\geqslant 1100$ K are difficult to perform with a high accuracy. To avoid these problems and to make the undercooled regime more accessible to calorimetric investigations, Fecht and Johnson [5] proposed application of modulation calorimetry under containerless processing conditions by modulating the heating power input from a radio frequency (rf) electromagnetic field to a levitated specimen combined with contactless pyrometric temperature measurement. Experimental tests of this method performed with solid Nb samples proved the feasibility of the method [6].

In the present study, the specific heat in the stable and undercooled melt of eutectic $ZrNi_{36}$, $ZrFe_{24}$, and $ZrCo_{23.5}$ alloys with melting points of 1283, 1230, and 1230 K, respectively, has been investigated in microgravity experiments. These alloys form the basis of the more complex "bulk" glass formers [11] and have been widely studied in the context of metastable phase formation [12]. However, no accurate experimental values of the specific heat in the stable and undercooled melt are available.

The experiments were performed in the containerless processing device TEMPUS [13], specifically designed for thermophysical experiments in microgravity. Microgravity conditions are necessary for this experiment to avoid excessive heating effects associated with levitation under 1-g conditions thus allowing processing under ultrahigh vacuum conditions and a high degree of liquid undercooking. This experimental procedure further ensures stable quiescent specimen conditions by the absence of the large stirring forces resulting from levitation under 1-g conditions.

2. METHOD

2.1. Heating Power Modulation

Based on the early work by Sullivan and Seidel [1], modulation calorimetry has been widely applied. A recent review is given in Ref. 3. In the containerless processing device TEMPUS [13] the specimen is heated by a 400-kHz dipole rf field (referred to as the heater) and positioned by a 200-kHz quadrupole rf field (referred to as the positioner) in the center of the heating coil. The total heating power input to the specimen is given by

$$P_{\text{tot}} = \rho(T) \int_V j^2 \, dv = P_{\text{H}} + P_{\text{Pos}} \tag{1}$$

where $\rho(T)$ is the resistivity and j is the current density induced by the magnetic field, H, of the heating coils. The difference in frequency and geometry of the dipole and quadrupole fields allows one to separate the total power input into additive contributions of the heating, P_{H}, and positioning fields P_{Pos}. The specimen is heated in a spherical outer shell of thickness $\delta = 5.032 \sqrt{\rho(T)/f}$ cm, with $\rho(T)$ in $\mu\Omega \cdot$ cm and the rf frequency f, in Hz. The positioning field is kept constant while temperature control and heating power modulation are accomplished by changing the heater field. For a spherical specimen of radius $R(T)$ the heater power input is given by [14, 15]

$$P_{\text{H}} = 3\pi P(T) \, \rho(T) \, F(x) \, H^2 \tag{2}$$

with $H^2 = L_{\text{H}} I_{\text{H}}^2$, where I_{H} is the current in the heating coils. $F(x)$ is a correction function accounting for the skin effect, with $x = R(T)/\delta(T)$. L_{H} is a purely geometric term depending on the relative positions of heating coils and specimen. Due to the mutual inductance between the specimen and the heater coils, I_{H} depends on the specimen resistivity and diameter [16]. The above equation is important for scaling of P_{H} as a function of I_{H}. We assume that at a calibration temperature T_c the heater power input is known for a given I_{H}. To obtain P_{H} at a different I_{H} the temperature dependence of the prefactor in Eq. (2) must be known. We define the heater coupling coefficient at

$$G_{\text{H}}(T) = 3\pi R(T) \, \rho(T) \, f(x) \, L_{\text{H}} \tag{3}$$

In a similar way, the coupling coefficient of the positioning field is defined as

$$P_{\text{Pos}} = G_{\text{P}}(T) \, I_{\text{Pos}}^2 \tag{4}$$

The temperature dependence of $G_H(T)$ and $G_P(T)$ is dominated by the change in resistivity and specimen radius at the melting point. For a given diameter, the ratio $G_H(T)/G_P(T)$ is a temperature-independent instrument parameter. The scaling with temperature will be the same; i.e., $G_H(T)/G_H(T_c) = G_P(T)/G_P(T_c)$. The equilibrium temperature, T_o, is determined by the Stefan–Bolzmann law:

$$A(T_o)\,\sigma\varepsilon(T_o)\,T_o^4 = G_H(T_o)\,I_{Ho}^2 + G_P(T_o)\,I_{Pos}^2 \tag{5}$$

where A, σ, and $\varepsilon(T_o)$ are the surface area, Stefan–Boltzmann constant, and total hemispherical emissivity, respectively. Heating power modulation is accomplished by modulating the oscillating circuit voltage of the heater with frequency ω. From the resulting heater current

$$I_H(t) = I_{Ho} + I_m \sin(\omega t) \tag{6}$$

the power input of the heater to the specimen is obtained as

$$P_H(t) = P_{Ho} + \Delta P_{av} + P(\omega)\sin(\omega t) + \Delta P_{av}\sin(2\omega t)) \tag{7}$$

The corresponding stationary temperature response consists of two phase-shifted modulation terms,

$$T(t) = T_o + \Delta T_{av} + \Delta T_m(\omega)\sin(\omega t + \phi_1) + \Delta T_m(2\omega)\sin(2\omega t + \phi_2) \tag{8}$$

with amplitudes $\Delta T_m(\omega)$ and $\Delta T_m(2\omega)$ and an increase in the average temperature, ΔT_{av}. Inspection of Eqs. (6) and (7) shows that the amplitudes of power modulation and the increase in average input power can be expressed as

$$P(\omega) = 2\sqrt{2}\,[P_{Ho}\,\Delta P_{av}]^{0.5} = 2G_H(T)[I_{Ho}I_m] \tag{9a}$$

$$P(2\omega) = \Delta P_{av} = \tfrac{1}{2}G_H(T)\,I_m^2 \tag{9b}$$

2.2. Thermal Analysis

Thermal analysis is conveniently performed in terms of thermal conductances coupling the specimen to the heater, heat bath, and thermometer [1]. To a first approximation, the specimen is uniformly heated in a spherical outer shell of thickness $\delta(T)$ and heat capacity C_H. This outer shell is considered as the heater, which is coupled to the inner part of the specimen with heat capacity C_S by a thermal contact resistance. The heater surface is radiatively coupled to a heat bath at ambient temperature. In the temperature range of our experiments and using measured values of the specimen resistivity, the skin depth δ ranges from $\delta = (8.7\text{–}9.9)\ 10^{-2}$ cm,

amounting to a directly heated volume fraction of 51 to 57%. Temperature is measured at the specimen surface by a pyrometer and thus corresponds to the heater temperature. The thermal coupling between specimen and thermometer and additional electronic relaxation times of the pyrometer can be neglected [5]. Following the model outlined above and considering the case where the amplitude of the resulting temperature variation is much smaller than the equilibrium temperature T_o, we obtained

$$C_H \frac{dT_H}{dt} = P(\omega)\sin(\omega t) + P(2\omega)\sin(2\omega t) + \Delta P_{av} - K_H[T_H(t) - T_S(t)] - K_B T_H(t) \tag{10a}$$

$$C_S \frac{dT_H}{dt} = K_H[T_H(t) - T_S(t)] \tag{10b}$$

$T_S(t)$ and $T_H(t)$ refer to the deviation of heater and specimen temperature from T_o, respectively. K_H represents the heater–specimen and K_B the heater–bath thermal conductance, with corresponding relaxation times $\tau_{ij} = C_i/K_j$. Solving for $T_H(t)$, the steady-state amplitude of temperature modulation at frequency ω, ΔT_m, and the increase in the average temperature, ΔT_{av}, are obtained as

$$\Delta T_m = f(\omega, \tau_1, \tau_2)\frac{P(\omega)}{C_P \omega} \tag{11a}$$

$$\Delta T_{av} = \Delta P_{av}\frac{\tau_1}{C_P} \tag{11b}$$

with $C_P = C_H + C_S$. The modulation component at 2ω results in a term similar to Eq. (11a) with ω replaced by 2ω. The correction function $f(\omega, \tau_1, \tau_2)$ takes into account the effects of the different relaxation times on the temperature response of the specimen. We first discuss the relevant time scales.

External Relaxation Time τ_1: Radiative Coupling to a Heat Bath at Ambient Temperature. τ_1 can be obtained from measurements of the specimen temperature following a step function change of the heater power [5, 6]. With the condition $\Delta T(t=0)/T_o \ll 1$, the external relaxation time is given by

$$\tau_1 = (C_H + C_S)/K_B = \frac{C_P}{4A(T_o)\,\sigma\varepsilon T_o^3} \tag{12}$$

resulting in an exponential time dependence of the temperature change $\Delta T(t)$ as a result of a step function change in heater power. Measurements of external relaxation times have been used in low-temperature experiments for very precise determination of heat capacity [18]. Here the procedure can be inverted to obtain the total hemispherical emissivity from combining modulation calorimetry with τ_1 measurements. It is important to point out that effects of the finite thermal conductivity can be detected in a deviation of $\Delta T(t)$ from purely exponential behavior [18]. In the temperature range of our experiment $\tau_1 \geqslant 18$ s.

Heater Specimen Relaxation Time τ_2. The uniformely heated outer shell of thickness $\delta(T)$ is coupled to the inner part of the specimen by a contact resistance K_H, resulting in a relaxation time

$$\tau_2 = C_H/K_H = \frac{C_H}{4\pi^3\kappa(R(T)-\delta(T))} \tag{13}$$

where κ is the thermal conductivity. Considering the measured values of the specific heat and electrical resistivity of liquid $ZrNi_{36}$ alloy at 1300 K and applying the Wiedemann–Franz law, this relaxation time is obtained as $\tau_2 < 0.1$ s for an 8-mm-diameter specimen.

Internal Relaxation Time τ_3. The finite thermal conductivity of the specimen can be described by an internal relaxation time τ_3 [5]:

$$\tau_3 = C_S/K_S = \frac{3C_S}{4\pi^3\kappa(R(T)-\delta(T))} \tag{14}$$

where K_S is the average thermal conductance of a sphere of radius $R-\delta$ and we can set $C_S \approx C_P(1-3\delta(T)/R(T))$. τ_3 represents the time scale of the decay of thermal gradients. τ_3 is obtained as $\tau_3 = 0.24$ s, which is small on a modulation time scale of 0.10 Hz.

The difference in τ_2 and τ_3 describing the same transport mode originates from the different areas through which heat is transported and thermal loads, C_H versus C_S, respectively. It is interesting to point out that the electrical resistivity contributes significantly to the temperature dependence and ratio of τ_2 and τ_3. Implicitly, the effect of the finite thermal conductivity is contained in the heater–specimen relaxation, Eq. (10b). To examine the time behavior of transient thermal gradients more closely, we calculated the decay of a thermal gradient imposed on the specimen surface from analytical solutions of the heat transport equation [19]. We observe that for our ZrNi specimen with a measured liquid resistivity at 1300 K of 145 $\mu\Omega \cdot$ cm, the center temperature is within 1% of the surface temperature after 1.4 s, corresponding to an effective internal relaxation time

of 0.3 s. Convection due to electromagnetically driven currents was not taken into account but will tend to shorten the internal relaxation time.

Two limiting cases of the correction function $f(\omega, \tau_1, \tau_2)$ are given below. (i) The low-frequency limit, characterized by $1/\Omega_m \gg \tau_2$, is entirely dominated by the external relaxation time τ_1:

$$f(\omega, \tau_1) = [1 + \omega_m \tau_1)^{-2}]^{-0.5} \tag{15a}$$

(ii) The high-frequency limit, characterized by $\tau_1 \gg \tau_2 \gg 1/\omega_m$, is given by

$$f(\omega, \tau_2) = \frac{C_H + C_S}{C_H} \tag{15b}$$

resulting in a modulation amplitude given just by the heat capacity of the directly heated volume fraction. The effect of thermal relaxation times on the measured temperature response can be neglected if the modulation frequency ω can be chosen such that [3]

$$(\omega\tau_1/10) > 1 > 10\omega\tau_3 \tag{16}$$

This adiabatic regime is characterized by a phase lag $\phi = 90°$ and $f(\omega, \tau_1, \tau_2) \approx 1$, equivalent to the condition $(\Delta T_m \omega) = \text{constant}$ as a function of ω. For a particular modulation frequency, the validity of the left-hand side can be directly inferred from τ_1 measurements. The internal relaxation time can, in principle, be measured from the highfrequency dependence of the temperature response. This requires a detailed heat flow model depending on the particular geometry [1, 20], i.e., the position of the heater and thermometer. As the validity of the Wiedemann–Franz law is well established for liquid metals [21], measurements of the electrical resistivity provide a good guideline for chosing the proper modulation frequency. In the TEMPUS device, these measurements could be performed *in situ* [22]. Furthermore, modulation calorimetry can be performed in the low-frequency regime, where corrections due to the finite τ_2 can be safely neglected while those due to τ_1 can be applied with a high accuracy.

3. EXPERIMENTS

3.1. Temperature Profile

The ZrNi, ZrCo, and ZrFe specimen used had a diameter of 8 mm, corresponding to a mass of typically 1.9 g. All test specimens were processed under UHV conditions. Temperature was measured with a two-channel InAs pyrometer with a sensitivity in the range of 1.8–2.8 and

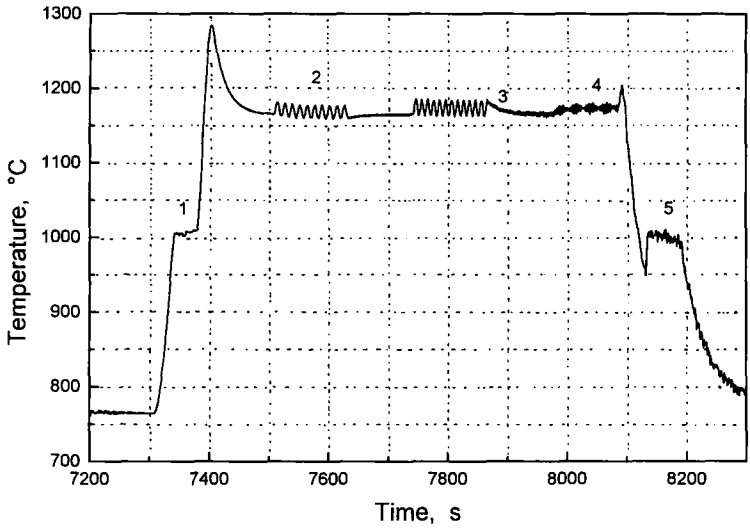

Fig. 1. Typical experiment sequence on $Zr_{64}Ni_{36}$ conducted during the space mission showing the specimen temperature as a function of time. The temperature corresponds to readings from the InAs pyrometer.

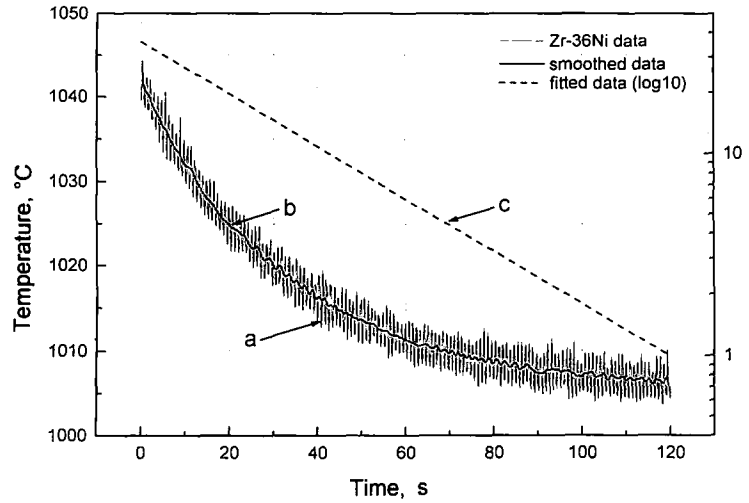

Fig. 2. Temperature relaxation following a step function change of the heater power. Curves a and b; left-hand ordinate: (a) raw data and (b) smoothed data. Curve c; righthand ordinate: logarithmic plot of smoothed data after baseline subtraction.

3.0–4.0 μm. The pyrometer was calibrated for each sample in ground-based experiments on solid specimens and in situ at the melting point.

Measurements were performed in the stable and 30 K undercooled melt. The maximum undercooling obtained at radiative cooling rates of $\approx 30\ \mathrm{K\,s^{-1}}$ was 82 K. Figure 1 shows the result of a typical experimental run for ZrNi performed in the space experiment. Starting from a crystalline specimen five steps are clearly discerned: (i) the melting plateau, overheating, temperature equilibration in the stable melt; (ii), iv modulation calorimetry at different frequencies showing the increase in the average temperature; (iii) decay to equilibrium temperature with time constant τ_1 at the end of a modulation sequence; and (v) undercooling and recalescence plateau. Five independent pieces of calorimetric information can be obtained from this sequence. (i) The enthalpy of fusion can be determined from the melting and recalescence plateau, (ii) the specific heat can be obtained from modulation experiments and from the increase in the average temperature, (iii) variation of the modulation frequency allows the determination of an internal relaxation time, (iv) the total hemispherical emissivity can be obtained from measurements of the external relaxation time, and finally, (v) an average value of the specific heat in the undercooled melt can be obtained from measurement of the duration of the isothermal recalescence plateau as a function of undercooling. Figure 2 shows the result of a typical τ_1 measurement for a ZrNi specimen at a bias temperature of 1280 K. The superimposed oscillations, curve a, result from movement in the potential well of the positioning field with eigenfrequencies near 1.8 Hz. Curve b shows smoothed data obtained from application of a FFT filter. Curve c shows a logarithmic plot of the smoothed data. No deviation from exponential behavior is seen, resulting in an external relaxation time of $\tau_1 = (33.1 \pm 0.2)$ s and a typical ratio of $\tau_1/\tau_2 > 90$.

3.2. Calibration Procedure

Quantitave evaluation of the heat capacity from measured temperature oscillations requires knowledge of $P(\omega)$. Calibration experiments were performed *in situ* by modulation calorimetry with solid specimens typically at $T_c = T_m - 50$ K. The specific heat at T_c was determined independently by conventional differential scanning calorimetry as $32.0\ \mathrm{J \cdot mol^{-1} \cdot K^{-1}}$ [23]. The appropriate modulation frequency at T_c was determined in ground-based measurements of the frequency dependence of ΔT_m [24]. Figure 3 shows the results of such a measurement in the form $(\Delta T_m \omega)$ as function of ω normalized to unit I_m. The condition $(\Delta T_m \omega) = \text{constant}$ results in a modulation frequency $\omega < 0.10$ Hz. The correction function

$f(\omega, \tau_1, \tau_2)$ was evaluated from τ_1 and resistivity measurements as $1 - f(\omega, \tau_1, \tau_2) \leqslant 0.01$ for $\omega = 0.10$ Hz. Consequently, we have chosen $\omega = 0.08$ Hz at T_c. The presence of the modulation component at 2ω requires a correction of $+6\%$ to the measured ΔT_m. From Eq. (11a) we obtain $P(\omega)$ at the calibration point, allowing us to determine $G_H(T_c)$. In a similar way, ΔP_{av} can be obtained from measurements of ΔT_{av} and τ_1 to give an independent evaluation of $G_H(T_c)$. Results obtained with both calibration modes agree within 5%, which is attributed to the overall measurement precision. It should be pointed out that measurements of ΔT_{av} are not affected by the internal relaxation time. The total hemispherical emissivity at the calibration point is obtained as $\varepsilon = 0.297$; this permits determination of the total radiant power P_{tot}. This calibration procedure has the advantages that (i) no knowledge of the emissivity is required (ii) $G_H(T_c)$ can be determined in the presence of a second heating field, and (iii) as the main contribution to the temperature dependence of $G_P(T)$ originates from the change at the melting point, it is rather insensitive to the absolute accuracy of pyrometric temperature measurement at a level of ± 20 K.

The positioner coupling coefficient $G_P(T_c)$ can be evaluated from power balance according to Eq. (5). Alternatively, modulation calorimetry can be used to obtain P_{Pos}. Qualitatively, Eqs. (9a), (9b), (11a), and (11b)

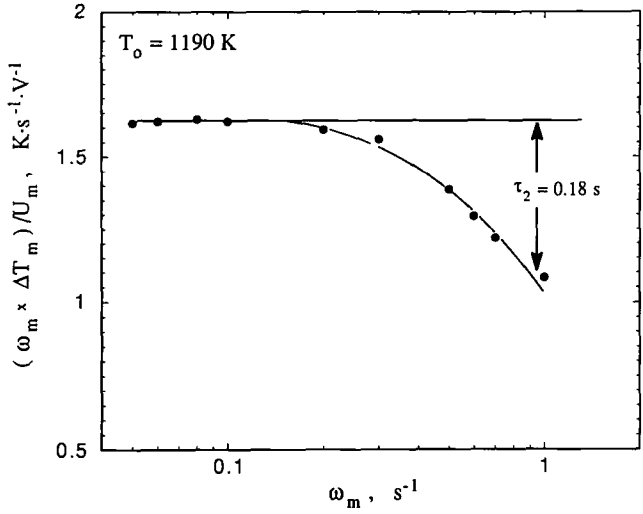

Fig. 3. Dependence of the temperature response ΔT_m on the modulation frequency for a solid 8-mm-diameter $Zr_{64}Ni_{36}$ sphere. The decrease in $(T_m \times \omega)$ for modulation frequencies >0.20 Hz is caused by the finite thermal conductivity of the specimen.

allow us to relate ΔT_{mod}, ΔT_{av}, and the bias temperature T_o. Writing the total power input as $P_{tot} = P_{Ho}(1+\alpha)$ with $\alpha = P_{Pos}/P_{Ho}$, we obtained

$$\Delta T_m^2 = 2f(\omega, \tau_1, \tau_2) \frac{1}{(\omega\tau_1)^2} \left(\frac{1}{1+\alpha}\right) T_{av} T_o \tag{17}$$

allowing us to determine the ratio P_{Pos}/P_{Ho}. With P_{Ho} known from modulation calorimetry, we can evaluate the coupling coefficient $G_P(T_c)$. We obtain a ratio of $G_H/G_P = 26.0 \pm 0.8$. A knowledge of the positioner heating efficiency is important for the evaluation of melting enthalpies and of the average heat capacity in the undercooked melt. With G_H/G_P fixed and temperature independent, Eq. (17) represents a consistency relation for the pyrometric temperature measurement.

To apply this calibration procedure to specific heat measurements at different temperatures and phases, the corresponding change in resistivity and radius must be known. It has been shown recently that it is possible to obtain the resistivity and, in particular, its change at the melting point directly from measurements of the oscillating circuit voltage and current in the space experiment using models of mutual inductance [22]. Thermal expansion in the solid and liquid state and the volume change upon melting have recently been measured for a typical glass forming alloy [25], giving a volume change of 3% at the melting point. An upper limit for the volume change at T_m can be obtained from the analysis of video recordings performed during the experiment.

4. RESULTS

The Main emphasis of the experiments was on measurements of the specific heat, c_p, in the stable and undercooled melt. In Table I, results obtained from modulation experiments with liquid $ZrNi_{36}$ are shown in some detail. Results from modulation experiments (m) and from measurement of ΔT_{av} and τ_1 (a) are shown in columns 3 and 4, respectively. At elevated temperatures, ΔT_{av} decreases relative to ΔT_m due to the decrease in the external relaxation time causing a larger error in ΔT_{av} measurement compared to ΔT_m. Within the indicated error, there appears to be no systematic difference in the specific heat values obtained with both methods. The c_p values shown in Table I have been scaled with a change in coupling coefficients of +6.7% at the melting point. Corrections due to τ_1 and τ_2 are $\leqslant 2\%$ in the entire parameter range used, resulting in a good agreement between c_p values obtained for modulation frequencies of 0.05 and 0.08 Hz. Depending on the modulation frequency, a further correction due to the presence of the modulation component at 2ω was applied. These

Table I. Experimental Results of Specific Heat Measurements on Liquid $Zr_{64}Ni_{36}$

T_o (°C)	ω_m (Hz)	c_p (m) ($J \cdot mol^{-1} \cdot K^{-1}$)	c_p (a) ($J \cdot mol^{-1} \cdot K^{-1}$)	ε_{tot}
1215	0.05	43.7 ± 0.8	43.0 ± 2	0.37
1160	0.08	44.5 ± 1.2	43.0 ± 4	0.35
1160	0.10	43.2 ± 1	43.5 ± 2	
1038	0.05	43.1 ± 1	41.2 ± 2	0.33
1038	0.08	43.0 ± 1	43.9 ± 2	
1008	0.05	44.0 ± 1	44.7 ± 2	0.33
1008	0.08	44.6 ± 1	45.7 ± 2	
980	0.05	45.5 ± 1.2		
960, solid, T_c	0.08	32.0 ± 1	32.0 ± 1	0.30

corrections were obtained from model calculations of the thermal response, resulting in a change of measured c_p values of $+2$ to $+2.5\%$. Values of the total hemispherical emissivity obtained from τ_1 measurements and Eq. (12) are shown in Table I, column 5. $\varepsilon(T)$ scales to within 4% according to $\varepsilon - \sqrt{\rho T}$ as expected from the free electron model.

An estimate of the thermodynamic functions in the undercooked melt can be obtained from a linear extrapolation of the specific heat in the stable and undercooled melt. This requires a knowledge of the melting enthalpy, which was evaluated from the duration of the recalescence plateau at a minimum undercooking of 10 K as $\Delta H_f = 14.7$ kJ $\cdot$ mol^{-1}. The entropy difference $\Delta S^{lx}(T)$ was calculated to give an ideal reduced glass transition temperature, $T_{gr} = T_{go}/T_m$, according to the Kauzmann criterion, $\Delta S^{lx}(T_{go}) = 0$ of $T_{gr} = 0.52$, in good agreement with an experimental upper limit of $T_{gr} = 0.51$ obtained from DSC measurements on rapidly quenched splats [26] and a theoretical prediction from MD calculations of $T_{gr} = 0.49$ [27].

5. SUMMARY

We have demonstrated the quantitative application of contactless modulation calorimetry to measurements of the specific heat of liquid metallic specimens. Calibration procedures have been devised based on measurements in the solid state, scaling of the coupling coefficients according to the temperature dependence of the resistivity and thermal expansion, and choice of a modulation frequency in accordance with constraints set by the internal and external relaxation times. In addition, the method allowed evaluation of the enthalpy of fusion and of the total hemispherical emissivity. With these results, the thermodynamic functions in the undercooled melt

were estimated and suggest a reduced ideal glass transition temperature, i.e., a limit for maximum undercooking at 52% of the eutectic temperature for $ZrNi_{36}$.

ACKNOWLEDGMENTS

We acknowledge stimulating discussions with Prof. G. Frohberg of TU-Berlin, Dr. Bill Hofmeister of Vanderbilt University, Prof. W. L. Johnson of Caltech, and Dr. G. Lohöfer of the German Space Establishment DLR in Cologne. The excellent support from the MUSC team at DLR Cologne is acknowledged. We gratefully acknowledge the support from DARA Grant 50 WM 94-31-4

REFERENCES

1. P. F. Sullivan and G. Seidel, *Phys. Rev.* **173**:679 (1968).
2. P. Handler, D. E. Mapother, and M. Rayl, *Phys Rev. Lett.* **19**:356 (1967).
3. Y. A. Kraftmakher, in *Compendium of Thermophysical Property Measurement Methods, Vol. 1* (Plenum, New York, 1984), pp. 591–641; in *Specific Heat of Solids* (Hemisphere, New York, 1988), p. 299.
4. Y. A. Kraftmakher, *High Temp. High Press.* **24**:145 (1992).
5. H.-J. Fecht and W. L. Johnson, *Rev. Sci. Instr.* **62**:1299 (1299).
6. R. K. Wunderlich and H.-J. Fecht, *Appl. Phys. Lett.* **62**:3111 (1993).
7. D. M. Herlach, R. F. Cochrane, I. Egry, H.-J. Fecht, and A. L. Greer, *Int. Mat. Rev.* **38**:273 (1993).
8. E. Schwarz, G. Jacobs, and S. Sauerland, *Int. J. Thermophys.* **17** (1996).
9. F. Spaepen, *Acta. Metall.* **23**:729 (1975).
10. C. V. Cochrane and F. Spaepen, *Acta. Metall.* **27**:1885 (1979).
11. A. Peker and W. L. Johnson, *Appl. Phys. Lett.* **63**:2342 (1993).
12. R. Bormann and K. Zölzer, *Phys. Stat. Sol.* **131**:691 (1992).
13. Team Tempus, *Containerless Processing in Space, Recent Results* (Lecture Notes in Physics, Springer Verlag, Berlin, 1995).
14. E. Fromm and H. Jehn, *Z. Metallkd.* **56**:599 (1965).
15. E. Fromm and H. Jehn, *Z. Metallkd.* **58**:366 (1967).
16. N. El-Kaddah and J. Szekely, *Metall. Trans.* **14B**:401 (1983).
17. R. K. Wunderlich, A. Diefenbach, R. Willnecker, and H.-J. Fecht, *Containerless Processing: Techniques and Applications*, W. L. Hofmeister, ed. (Minerals, Metals & Materials Society, 1993).
18. R. D. Bachmann, F. J. Di Salvo, T. H. Geballe, R. L. Greene, R. E. Howard, C. N. King, H. C. Hirsch, K. N. Lee, R. E. Schwall, H. U. Thomas, and R. B. Zubeck, *Rev. Sci. Instr.* **43**:205 (1972).
19. Carslaw and Jaeger, *Conduction of Heat in Solids* (Oxford University Press, Oxford, 1959) pp. 230–238.
20. R. K. Wunderlich *et al.*, in press.
21. T. Iida and R. I. L. Guthrie, *The Physical Properties of Liquid Metals* (Clarendon Press, Oxford, 1993), pp. 226–237.
22. G. Lohöfer, in press.

23. R. Wilde, personal communication.
24. R. K. Wunderlich and H.-J. Fecht, in *Ninth European Symposium, Gravity Dependent Phenomena in Physical Sciences*, Berlin, Germany, May (1995).
25. H.-J. Fecht, S. G. Klose, and M. P. Macht, *Proceedings of the 2nd Pacific Rim International Conference on Advanced materials and Processing*, K. S. Shin and S. J. Kim, eds. (Korean Institute of Metals and Materials, 1995) p. 2155.
26. K. H. J. Buschow, B. H. Verbeek, and A. G. Dirks, *J. Phys. D* **14**:1087 (1981).
27. T. Aihara, Jr., K. Aoki, and T. Masumoto, *Mat. Trans. JIM* **36**:399 (1995).